CLM - P72

United Kingdom Atomic Energy Authority

RESEARCH GROUP

Preprint

HYDROMAGNETIC WAVES IN A PARTIALLY IONIZED HYDROGEN PLASMA

A. MALEIN

Culham Laboratory,

Culham, Abingdon, Berkshire

1965

UNCLASSIFIED
(Approved for Publication)

CLM - P 72

HYDROMAGNETIC WAVES IN A PARTIALLY IONIZED HYDROGEN PLASMA

by

A. MALEIN

(Submitted for publication in 'Nuclear Fusion')

A B S T R A C T

This paper gives further experimental verification of the theory of fast hydromagnetic waves.

By a suitable choice of plasma conditions the compressional wave is propagated in a partially ionized cylindrical hydrogen plasma at frequencies below the ion-cyclotron frequency.

The propagation constants of the wave are measured experimentally by observing the phase velocity and attenuation over a fixed distance. Other plasma parameters, with the exception of the neutral density are measured independently.

In order to obtain good experimental agreement with the theoretical curves computed from the measured data, it is necessary to postulate a considerable neutral particle density in the wave. This gives rise to loading of the wave, observable as a reduction in the Alfvén speed, and also to wave damping not explicable by resistive effects alone.

The enhanced loading produced by neutral particles is unaffected by variations in magnetic field and the fitted value of neutral density derived from wave cut-off data is in agreement with that calculated from attenuation measurements.

U.K.A.E.A. Research Group,
Culham Laboratory,
Nr. Abingdon,
Berks.

March, 1965 (C/18 IMG)

C O N T E N T S

1. INTRODUCTION

The theory of hydromagnetic waves in cylindrical plasmas has been investigated by many workers, in particular by WOODS [1] , whose theory has provided the basis for the present study.

The dispersion relation for hydromagnetic waves in a cylindrical plasma has two branches, corresponding to distinct modes of oscillation which we call the slow and fast waves. The slow wave propagates only at frequencies below the ion cyclotron frequency and is basically a torsional oscillation. In a bounded medium the fast wave propagates only if the angular frequency ω is greater than the limit set by the product $k_c V_A$, where k_c is the radial wave number and V_A is the Alfvén speed. The wave is compressional and if $\omega \ll \omega_{ci}$ has a phase velocity, $V_{ph} = \omega(\omega^2/V_A^2 - k_c^2)^{-\frac{1}{2}}$.

In our earlier work on the propagation of the fast wave in a cylindrical argon plasma [2] the cut-off frequency ($k_c V_A$) was greater than the ion cyclotron fre-frequency (ω_{ci}). In the present work we study waves of a frequency such that $k_c V_A < \omega < \omega_{ci}$. To meet this condition, $k_c V_A \ll \omega_{ci}$, we must have

$$\frac{k_c^2 B_o^2}{4\pi n_i m_i} \ll \frac{e^2 B_o^2}{m_i^2 c^2} \qquad \ldots (1)$$

$$k_c^2 \ll \frac{4\pi n_i e^2}{m_i c^2} \; . \qquad \ldots (2)$$

Now $k_c = \frac{Q}{r}$ where r is the radius of the cylinder and Q is a number depending upon the radial mode involved. Thus we obtain the criterion in terms of the line density of ions ($N = \pi r^2 n_i$) and the ion mass

$$\frac{4e^2 N}{m_i c^2 Q^2} \gg 1 \; . \qquad \ldots (3)$$

For the lowest mode in a conducting tube $Q = 3.7$ and we obtain,

$$\frac{N}{m_i} \gg 2 \times 10^{40} \; . \qquad \ldots (4)$$

In order to satisfy this criterion the gas is changed to hydrogen, reducing

the ion mass, but increasing the difficulty in obtaining a sufficiently quiescent plasma for the experiments. In fact we achieve parameters such that $\omega_{ci} \sim 10\ k_c V_A$.

Under similar conditions, GOULD [3] has described an experiment in which a pulse is excited and its frequency content, as a function of distance, is analysed to give values not only of the propagation constants but also of resistivity, ion density and ion neutral collision frequency. Independent measurements of the parameters involved were not made.

In this experiment a tuned exciter, which generates a single frequency, is used for measurement of the propagation constants, and all other parameters are measured separately, except for the neutral density which is fitted.

The conditions for the experiment are such that the ion-neutral collision frequency is higher than the wave frequencies used. Therefore, the damping of the wave is affected by neutral atoms in the plasma and these also contribute to the loading of the wave at lower frequencies.

2. APPARATUS

A diagram of the apparatus is shown in Fig.1. The discharge tube itself consists of a 22 cm bore Pyrex cylinder 250 cm long. The stainless steel electrodes are thin discs 20 cm in diameter, spaced 200 cm apart, having small central apertures to allow a laser beam to pass axially through the plasma column. This assembly is supported coaxially within a brass cylinder acting as a return current conductor. This has a longitudinal slit to permit B_z field penetration from a surrounding solenoid supplied by a 200 kJ capacitor bank. Peak fields up to 8 kG are possible with a rise time of 2 msec.

The gas discharge current is supplied by a 16 kJ capacitor bank, through an ignitron circuit providing switching and crow-barring functions. A pulse transformer with alternative ratios can be included in the circuit, allowing some variation in load impedance and current rise time.

A tightly fitting screen of brass mesh is fitted over part of the external

surface of the discharge tube; this provides conducting wall boundary conditions at wave frequencies without affecting more slowly varying fields.

3. WAVE EXCITATION

A wide range of experimental frequencies is desirable but we are limited by a lower cut-off frequency of about 500 kc/s at 4 kG, and at frequencies much above 2 Mc/s the wave amplitude becomes too small for accurate measurements. Both increased absorption and smaller stored energy in the capacitor at higher frequencies contribute to this restriction.

The exciter loop is a 7 cm wide aluminium strap tightly clamped round the Pyrex discharge tube at a distance 60 cms from the anode and about 20 cms from the section of the tube encased in the wave guide.

A low inductance line couples this loop to a series resonant circuit, contained in a screened enclosure and comprising a spark gap, incremental inductances and a selection of high frequency capacitors. The latter are arranged to give the larger variations in frequency. The circuit is normally charged to 20 kV and is triggered from a delay circuit controlling the axial field and discharge current switches.

4. WAVE DETECTION

Fig.2 shows oscillograms of the signals from two small coils separated by 12 cms and situated on the axis of the discharge tube. They are oriented to accept the $B_{1(z)}$ component of the wave field which is maximum at the centre where $B_1(r)$ and $B_1(\theta)$ are both zero. The coils have an effective area of 5 cm^2 and are shielded against electrostatic fields by slotted, thin-wall, stainless steel tubes. Quartz sheaths extend across a horizontal diameter of the tube through side ports which can also accommodate alternative diagnostic probes.

Experimental measurements are taken during the decaying portion of the wave envelope thus allowing time for any higher frequencies, generated as a transient response, to disappear.

The wave signals are not integrated, but a π-section low pass filter is used to suppress direct radiation from the spark gap at frequencies above 4 Mc/s.

The time taken for a particular wave peak to travel the distance between the two probes, and its reduction in amplitude, allow the phase velocity and the absorption coefficient to be calculated.

Because of the very high absorption experienced, no evidence of reflections from the end electrodes is seen.

Wave excitation seems more efficient at high magnetic fields and a value of 6 kG is used for most measurements involving other variables.

5. PLASMA PARAMETERS

The plasma parameters involved in the dispersion relation are the ion and neutral densities, the electrical conductivities parallel and perpendicular to the magnetic field and the ion neutral collision frequency. This last quantity depends upon the ion temperature and the cross section for momentum exchange as well as the neutral density. We assume that the ion temperature is equal to the measured electron temperature. Under the conditions of high ion density ($\sim 10^{15}$ cm^{-3}) and low temperature ($\sim$ 1 eV) in the plasma, this is a plausible assumption since the energy exchange time is $\sim$ 0.1 μsec. The cross section for charge exchange is taken from FITE's data for proton-atomic hydrogen collisions [4] . We assume $\sigma_\perp = \frac{1}{2}\sigma_\parallel$ and fit the neutral density to give best agreement for both real and imaginary propagation constants.

It is well known that in gas discharges of the type used here, the neutral density is not accurately given by the difference between the initial particle density and the ion density [2],[9]. In all the following discussion, n is taken as the initial gas filling density and n_o is the total particle density of ions and neutrals, $(n_i + n_n)$, in the plasma, at the time of wave propagation.

The wave experiments are carried out in an after-glow plasma and in a plasma carrying a considerable axial current. Some of the measurements of plasma

properties now to be mentioned, cannot be made in both cases.

(a) The value of the electrical conductivity is calculated from the measured value of T_e, using figures given by SPITZER [5]. If axial current is flowing, then $\sigma_{\parallel}$ can be calculated from the measured value of the electrostatic field and the current density. In a turbulent plasma this measurement has not been in close agreement with the value derived from T_e.

(b) A floating Langmuir double probe [6] is used to check the uniformity of the ion number density and the electron temperature. Probe characteristics are plotted at several different radial positions.

(c) The mean number density ($\bar{n}_e$) of electrons on the tube axis is determined by using the $H_e - N_e$ laser interferometer developed in this laboratory [7], and also by observing the Faraday rotation of a plane polarised 28 μ wavelength radiation produced by a short pulse water vapour laser. The attenuation of this laser beam in passing through the plasma provides an independent check on the value of T_e [8].

(d) The number density of the neutral atoms in the plasma is not known and cannot be measured directly, neither can we assume that the percentage ionization is simply derived from n_i and the initial filling density, n.

We can estimate the likely value of the ion neutral collision frequency (ν_{in}) under typical plasma conditions. The collision frequency is given approximately by $\nu_{in} = n_n \sigma_{xc} v_i$. The initial atom number density corresponding to a hydrogen pressure of 200 mTorr is $n = 1.46 \times 10^{16}$ cm^{-3} and if our measured value of n_e is about 4×10^{15} cm^{-3} we can say that $n_n \sim 10^{16}$ cm^{-3}.

If we assume $T_i \leqslant T_e = 1$ eV then $v_i \leqslant 1.7 \times 10^6$ cm/sec. The momentum transfer cross section (σ_{xc}) for 1 eV protons is approximately 3×10^{-15} cm^2 [4].

We obtain $\nu_{in} \sim 5 \times 10^7$ sec^{-1}, and even if n_n is reduced by an order of magnitude due to particle loss, the frequency is still above the experimental range, so that collisions between ions and neutrals will be an important process affecting wave propagation.

6. PLASMA PRODUCTION

6.1 Afterglow Plasma

We find that the same ionizing current waveform which produces a steady plasma in argon [2], gives us a very unstable plasma in hydrogen.

We judge whether the plasma is initially suitable for wave measurements by examining the regularity of the laser fringe pattern and Fig.3(a) shows the ionizing current waveform and the associated fringe pattern in an argon plasma at 50 mTorr. In hydrogen, even at a pressure of 200 mTorr only a few recognisable fringes appear towards the end of the pulse. Full ionization would produce nearly 90 fringes.

Various changes in the discharge circuit result finally in the current waveform shown in Fig.3(b) where the capacitor bank is short circuited at peak reverse voltage by an ignitron shown by broken lines in Fig.1. Only when axial current ceases at the end of the first half cycle do smooth fringe patterns appear.

The wave is excited at a time 50 μsec after the start of this quiet phase, when the average value of n_e is $2.0 \pm 0.1 \times 10^{15}$ cm^{-3}.

This afterglow plasma allows accurate measurements to be made with the double probe; the value of n_i is found to be $2.1 \pm 0.2 \times 10^{15}$ cm^{-3} and $T_e = 1.4 \pm 0.1$ eV. The ion density falls off to about half value within 2 cms of the tube wall.

The variation of the phase velocity and wave damping with frequency is measured at 4 kG and 6 kG at the time mentioned above, and also at 6 kG when $n_i = 1.4 \pm 0.1 \times 10^{15}$ cm^{-3}, 200 μsec later.

Because of the low ion density measured in the afterglow, the method of plasma formation was changed in later experiments.

6.2 High Current Plasma

We find that a short current pulse rising to about 40 kA in 35 μsec not only gives a higher percentage ionization but regular fringe patterns are produced soon

after current peak (see Fig.4).

The number of fringes indicates that the peak electron density is about 6×10^{15} cm^{-3} but the time at which the maximum occurs is variable from shot to shot. We choose a later time for wave propagation, 100 μsec after current peak when the variation is small and the average value of electron density is $n_e = 4.3 \pm 0.1 \times 10^{15}$ cm^{-3}. A subsequent measurement of Faraday rotation under identical plasma conditions gives a value $n_e = 4.3 \pm 0.8 \times 10^{15}$ cm^{-3}. Absorption of this 28 μ laser beam indicates that $T_e \lesssim 1.3$ eV.

The conductivity is calculated to be $\sigma_{\parallel} = 53\ \Omega^{-1}$ cm^{-1} (SPITZER) taking $T_e = 1.4$ eV and this value is used throughout for computation of theoretical curves. The effect of an error in this quantity is discussed later. In general, attempts to measure $\sigma_{\parallel}$ in the plasma have resulted in lower values.

7. THE DISPERSION RELATION

For the experimental plasma parameters given above the pressure and viscosity terms in the dispersion relation, equation (27) of WOOD's theoretical treatment, are negligible, allowing us to use the simpler form, equation(60). [1] .

This dispersion relation which we solve numerically is,

$$\left\{Sk^2 - k_A^2\left(1 + \frac{ik^2}{\sigma_\perp \omega} + \frac{ik_c^2}{\sigma_{\parallel}\omega}\right)\right\}\left\{S(k^2 + k_c^2) - k_A^2\left(1 + \frac{ik^2}{\sigma_\perp\omega} + \frac{ik_c^2}{\sigma_\perp\omega}\right)\right\} = k^2(k^2 + k_c^2)\left(\frac{\omega}{\omega_{ci}}\right)^2$$

where

$$S = \frac{n_i - i\, n_n \frac{\omega}{\nu_{in}}}{n_i + n_n - i\, n_n \frac{\omega}{\nu_{in}}}$$

Note $S = 1$ when $n_n = 0$, $S \to \frac{n_i}{n_i + n_n}$ when $\omega \ll \nu_{in}$. k is the propagation constant, $\equiv \eta + i\varepsilon$ where η is axial wave number and ε is the absorption coefficient. k_c is the radial wave number, and $k_A = \frac{\omega}{V_A}$.

We excite only the lowest $m = 0$ mode, and measure $B_{1(z)}$, the perturbed axial field. $B_{1(z)} = A\, J_o(k_c r)$ where r is the radius of the tube and A is an amplitude factor.

The determination of the radial wave number k_c from boundary conditions has

been discussed fully by WOODS in his paper [1]. In this study we have taken that value corresponding to a uniform plasma reaching an effective conducting wall boundary at the inner tube radius. The effect of a non-uniform density distribution in which the variation with radius is of the form $n_i = n_{io} - cr^2$ has been considered by PATON and ROWLANDS (Private communication). The results show that to a first approximation the dispersion relation is unchanged, except that an effective value has to be taken for the ion number density, which is given by

$$n_i' = n_i - \frac{ca^2}{3}$$

where a is the radius of the plasma.

The density profile in our afterglow plasma suggests that we ought to take a value about 20% less than that measured on the axis.

Except for values of ω near cut-off when $\eta/\varepsilon \sim 1$ it is permissible to assume that k_c is a real number in the forgoing theoretical treatment.

8. THE DISPERSION CURVES

8.1 Afterglow Plasma

The dispersion of the hydromagnetic wave is examined under both plasma conditions by measuring the axial wave number $\eta = \omega/V_{ph}$ at different wave frequencies ω, with constant axial field B_o.

The curves in Fig.5 represent solutions for η as a function of ω, for $n_i = 2.0 \times 10^{15}$ cm^{-3} at 4 kG and 6 kG, and for $n_i = 1.4 \times 10^{15}$ cm^{-3} at 6 kG. The two ion densities correspond to a time interval of 200 μsec elapsing between the two sets of measurements.

Since the ion neutral collision frequency is so high the family of dispersion curves with varying percentage ionization coincide at low values of η, suggesting that near cut-off

$$V_A = \frac{B_o}{(4\pi m_i(n_i + n_n))^{\frac{1}{2}}}$$

and the effective wave loading is provided by both ions and neutrals. The value of $(n_i + n_n)$ is found to be much less than the initial filling density n, and so

the computed curves are those for $n_o = 8 \times 10^{15}$ cm^{-3} which gives satisfactory agreement at both times of propagation. It seems conclusive therefore that most particles are lost during the ionizing current phase.

The experimental points shown with their standard errors are averaged results of at least 20 measurements.

Records of individual waves taken simultaneously at different radial positions by a multiple probe, show a lack of symmetry, (Fig.6). The average of a number of such measurements gives a radial distribution which approximates to a J_o Bessel function but the large errors lead to a corresponding uncertainty in the value of k_c.

It is clear that as a smaller plasma radius would increase the value of k_c, the lowering of the cut-off frequency which we observe cannot be due only to this effect, but to a dominant reduction in V_A, caused by increased wave loading.

In considering these points we note that if wave loading is dependent upon the total density, then the effect of a radial variation in n_i, may be compensated by a complementary variation in n_n.

The very large shot-to-shot differences in wave amplitude do not allow good damping measurements to be made. The average value of ε for the experimental range is about 0.15 cm^{-1}. This very high value is in agreement with theoretical values of $\varepsilon = 0.126 - 0.240$ cm^{-1} over the same range. It is difficult under these severe conditions to assess the contribution made by resistive damping.

8.2 High Current Plasma

In the high current plasma the wave is propagated after the peak of the ionizing current when about 14 kA is still flowing. The plasma is almost certainly very turbulent but it is obvious from the clarity of the wave records and the laser interferometer fringe pattern, that the plasma is more uniform than before. Presumably the turbulent cells are now much smaller than the dimensions of the plasma and the laser beam traverses enough of these to give an integrated resultant phase shift. In the afterglow plasma large scale inhomogeneities which

developed during the slow ionizing pulse remained frozen into the magnetised plasma throughout the later phase.

Radial variation of the $B_{1(z)}$ component of the wave field now shows little asymmetry. The shot-to-shot reproducibility of the wave is good and the wave damping is less, allowing more accurate measurements to be made.

Fig.7 shows the B_o, I_z wave forms and a pulse indicating the time of wave excitation. The attenuation of the wave as a function of frequency is computed and in Fig.8(a) we see the affect of taking a value of $n_i = 4 \times 10^{15}$ cm^{-3} and a variable neutral particle density. Fig.8(b) illustrates the close fit of the experimental points to the curve for which the total particle density $(n_i + n_n) = 1.0 \times 10^{16}$ cm^{-3}.

By taking this value of n_o we see in Fig.9 that the corresponding experimental points for axial wave number (η) also agree with the theoretical curve. Computed also are curves for $n_i = 3 \times 10^{15}$ cm^{-3} and $n_i = 6 \times 10^{15}$ cm^{-3} for comparison.

By computing the curves for η and ε at conductivity values corresponding to $T_e = 1.4 \pm 0.4$ eV we see that the real part of the dispersion relation is insensitive to variations in this parameter. Fig.10 shows the magnitude of the effect upon the absorption coefficient. We are able to conclude that the neutral and resistive contributions to wave damping are about equal, by comparing the experimental curve with theoretical curve for very high conductivity.

9. ION - NEUTRAL LOADING

Using the method suggested by GOULD [3] we investigate the variation in cut-off frequency with axial magnetic field. Since the cut-off frequency, $\omega_o = k_c V_A$ and $V_A = B/(4\pi m_i(n_i + n_n))^{\frac{1}{2}}$ we can derive n_n from the slope of the ω_o, B curve.

The exciter circuit, normally of high Q, is critically damped and the resulting current pulse in the circuit excites a wave containing many frequencies. The higher frequencies have a correspondingly high group velocity and these reach the

measuring probe first, while the last frequency to appear is just above the cut-off frequency.

Fig.11 shows a plot of experimental points derived from measurements at different field values, together with curves appropriate to three wave loading densities. Again it is necessary to postulate substantial wave loading by the neutral gas to obtain agreement with theory.

10. CONCLUSIONS

1. Our measurements supplement those of GOULD, et al. in confirming the general form of the dispersion relation for this wave.
2. To obtain quantitative agreement with the real part of the dispersion relation it is necessary to assume the presence of a substantial number of neutral atoms, effectively loading the wave.
3. With the number of neutral atoms fitted to give agreement with the real part of the dispersion relation, good agreement is also obtained with the imaginary (damping) part. Just under half of the observed damping is due to ion-neutral collisions, the remainder is attributable to electron-ion collisions, resistivity.

11. ACKNOWLEDGMENT

The author wishes to thank Dr R.J. Bickerton for his help and encouragement in this work; also Mr C.F. Parker who made most of the experimental measurements.

12. REFERENCES

[1] WOODS, L.C. Hydromagnetic waves in a cylindrical plasma. J. of Fluid Mechanics, 13, (1962) 570.

[2] JEPHCOTT, D.F. and MALEIN, A. Experimental study of fast hydromagnetic waves in an argon plasma. Proc. Roy. Soc. A 278, (1964) 243.

[3] GOULD, R.W., SWANSON, D.G., HERTEL, R.H. Experimental study of compressional hydromagnetic waves. Phys. Fluids, 7, (1964) 269.

[4] FITE, W.L. Collisions of hydrogen ions with hydrogen atoms. Proc. 4th International Conference on Ionization Phenomenon in Gases (Uppsala 1959) North Holland Publishing Co., Amsterdam. IA (1960) 23.

[5] SPITZER, L. Physics of Fully Ionized Gases. Interscience Publishers, (1962) 139.

[6] JOHNSON, E.O. and MALTER, L. A floating double probe method for measurements in gas discharges. Physical Review, 80, (1950) 58.

[7] ASHBY, D.E.T.F., JEPHCOTT, D.F., MALEIN, A. and RAYNOR, F.A. Performance of the He - Ne laser as an interferometer for measuring gas density. J. of Applied Physics, 36 (1965) 29.

[8] DELLIS, A.N., EARL, W.F., MALEIN, A. and WARD, S. Far infrared Faraday Rotation in a Plasma. submitted to Nature.

[9] JEPHCOTT, D.F. and STOCKER, P.M. Hydromagnetic waves in a cylindrical plasma: an experiment. J. of Fluid Mechanics, 13 (1962) 587.

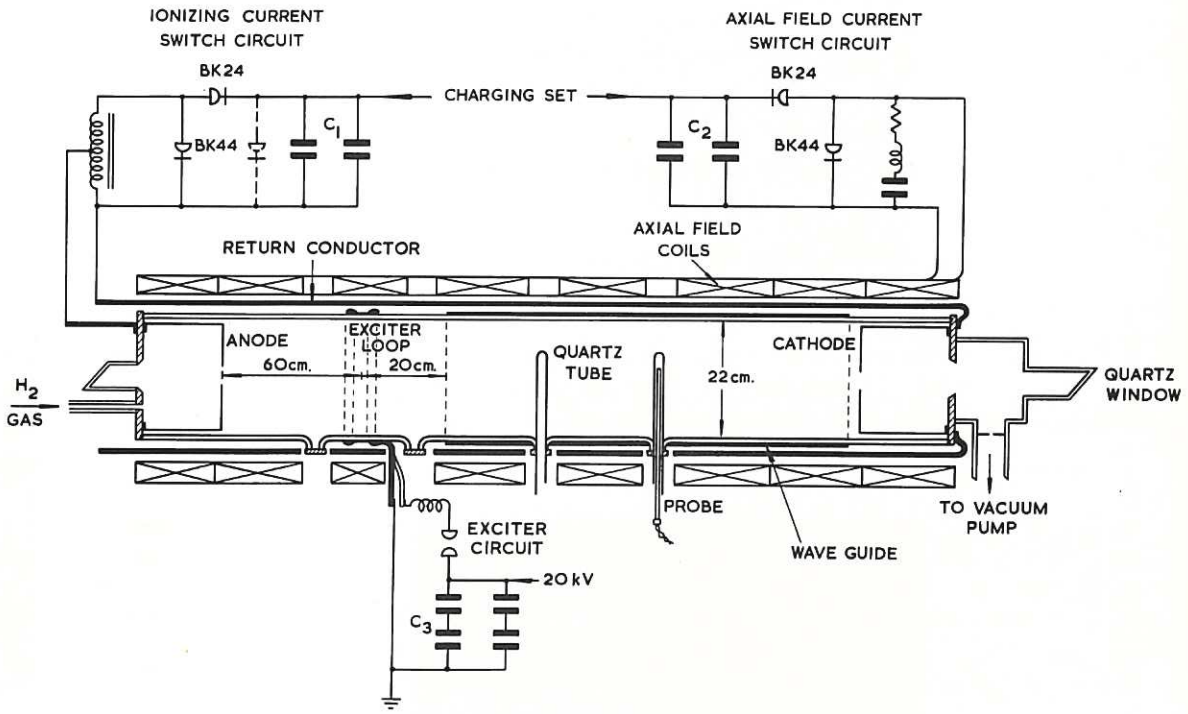

Fig. 1 (CLM-P72)
Experimental discharge tube and circuit details

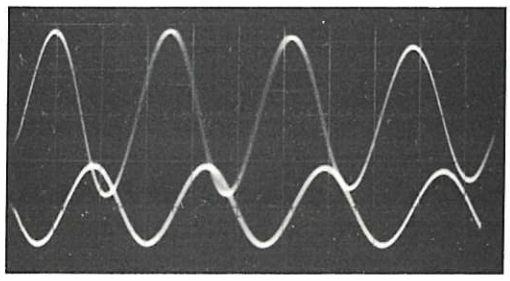

Fig. 2 (CLM-P72)
Magnetic probe signals - 12 cm probe spacing.
Upper trace 0.5 V/cm
Lower trace 0.2 V/cm
Sweep speed 0.5 μs/cm

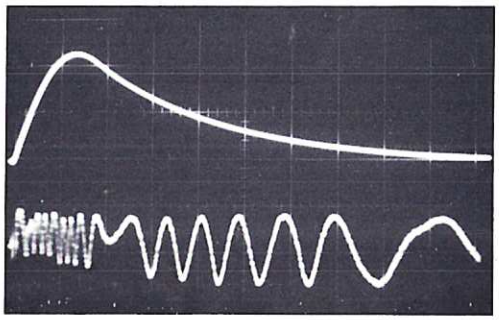

Fig. 3(a) (CLM-P 72)
Upper trace discharge current 10 kA/cm; Lower trace Laser interferometer fringe pattern at 3.4 μ; Sweep speed 100 μs/cm

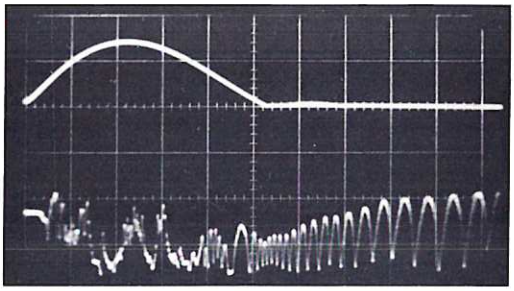

Fig. 3(b) (CLM-P 72)
Upper trace discharge current 15 kA/cm; Lower trace Laser interferometer fringe pattern at 3.4 μ; Sweep speed 50 μs/cm

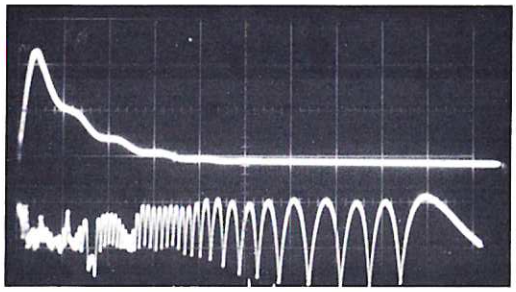

Fig. 4 (CLM-P 72)
Upper trace discharge current 20 kA/cm; Lower trace Laser interferometer fringe pattern at 3.4 μ; Sweep speed 100 μs/cm

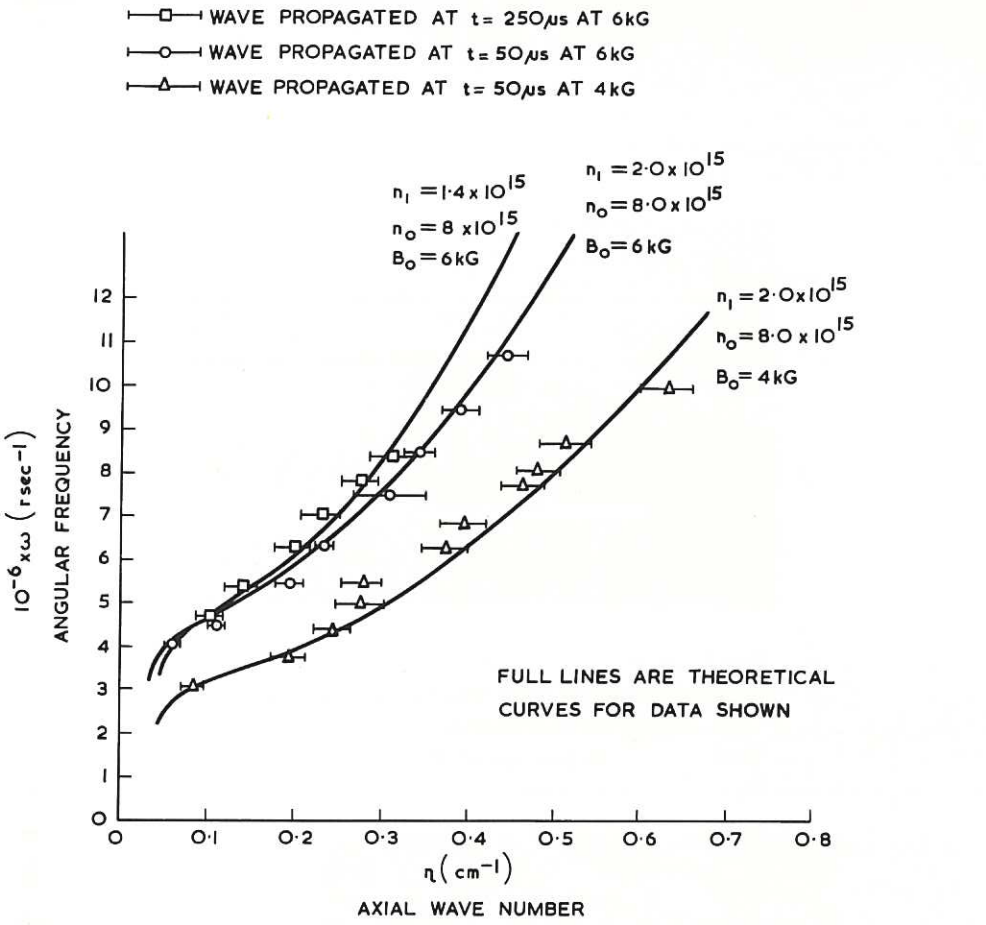

Fig. 5 (CLM-P 72)

Dispersion of the wave-afterglow plasma. Initial filling density $n = 1.46 \times 10^{16}\,cm^{-3}$; best fitted curves obtained with $n_0 = 8.0 \times 10^{15}\,cm^{-3}$

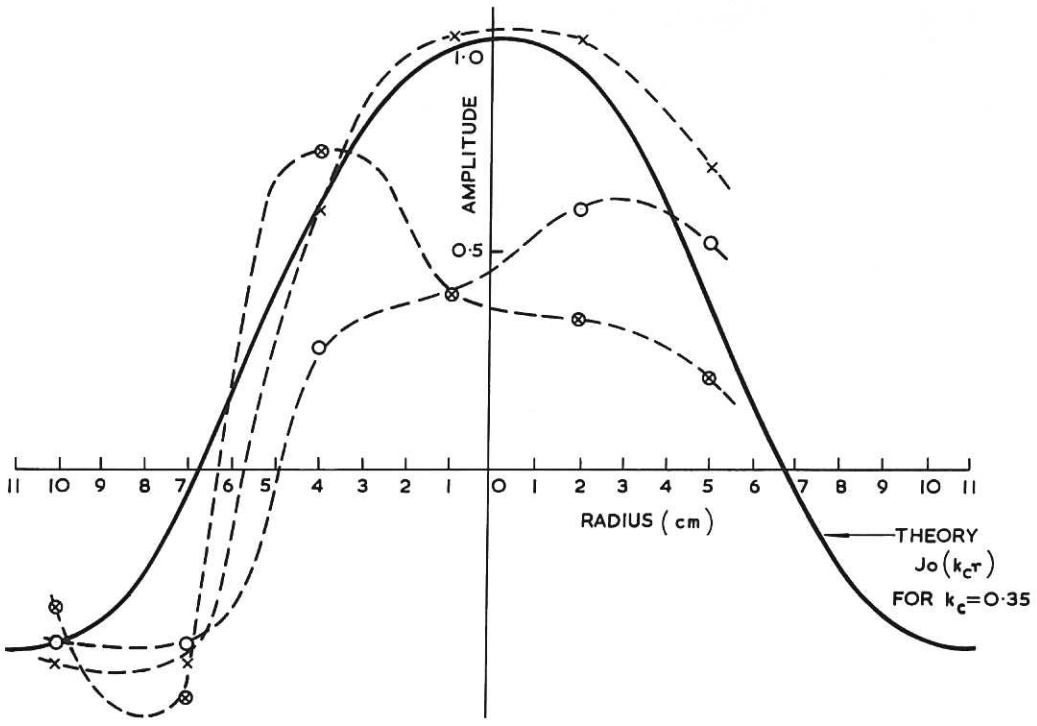

Fig. 6 (CLM-P 72)

Radial variation in amplitude of individual waves measured with a multiple probe in the afterglow plasma

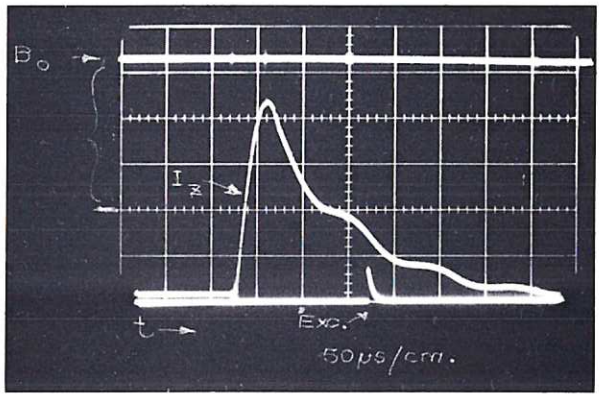

Fig. 7 (CLM-P 72)
Upper trace B_0 ; Lower traces, discharge current 10 kA/cm and exciter trigger pulse.
Sweep speed 50 μs/cm

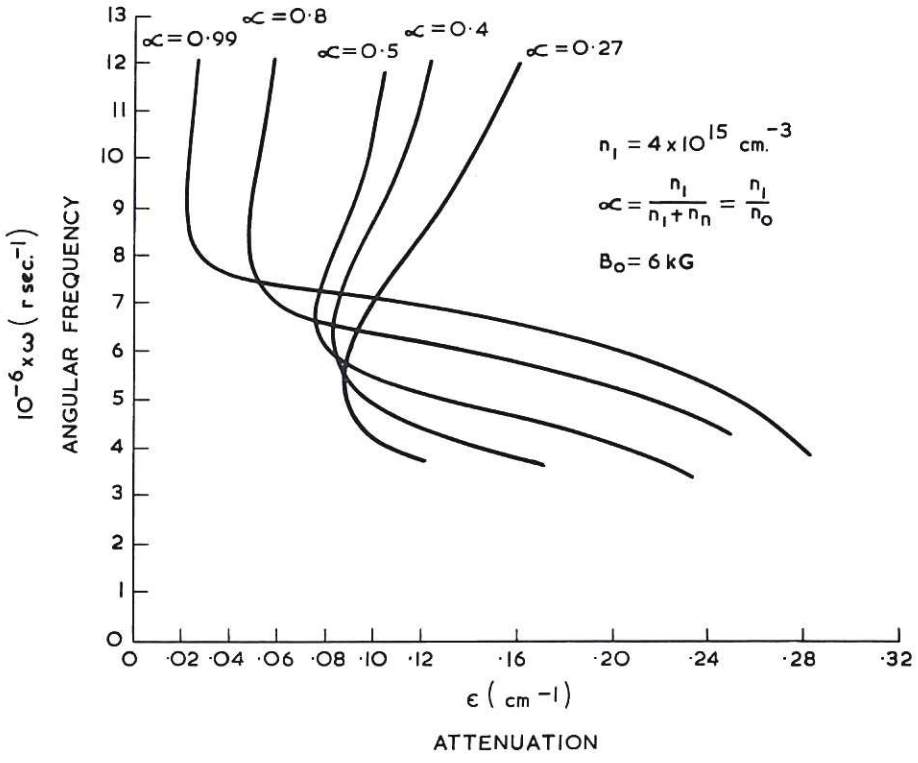

Fig. 8(a) (CLM-P 72)
Theoretical curves showing the dependence of the attenuation coefficient ϵ, upon the neutral particle density n_n, while the ion density remains constant at $n_i = 4.0 \times 10^{15}$ cm^{-3}

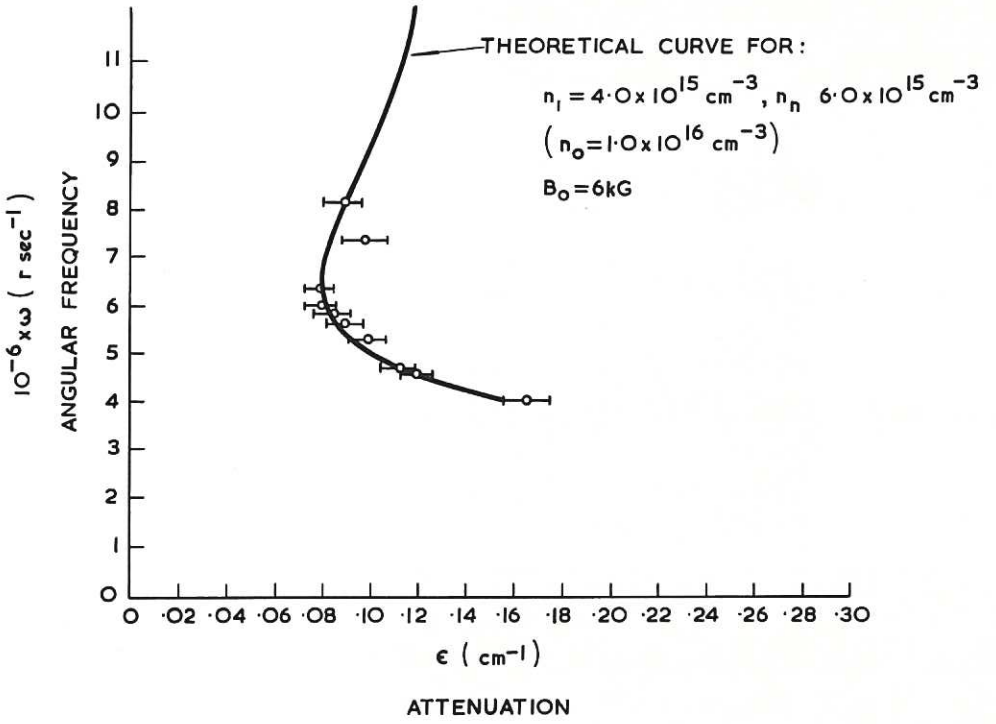

Fig. 8(b) (CLM-P72)
Wave damping - high current plasma n_n has been chosen to give the best fit to the experimental points

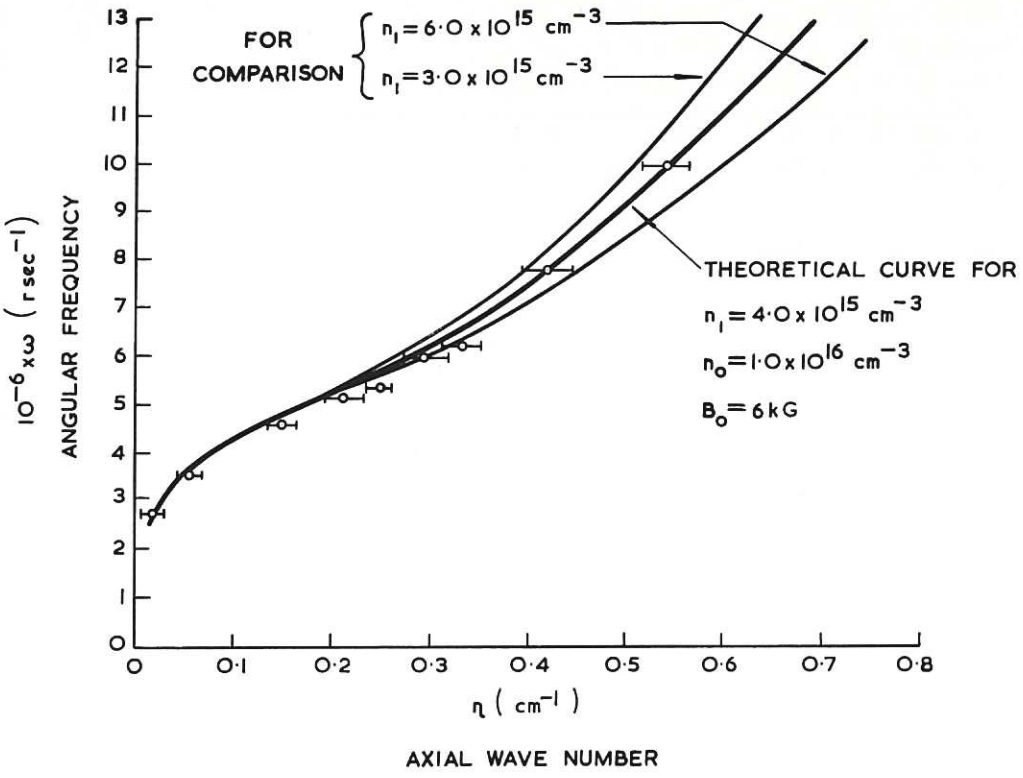

Fig. 9 (CLM-P72)
Dispersion of the wave - high current plasma. The theoretical dispersion curve is that corresponding to the damping curve fitted by choice of n_n in Fig. 8(b)

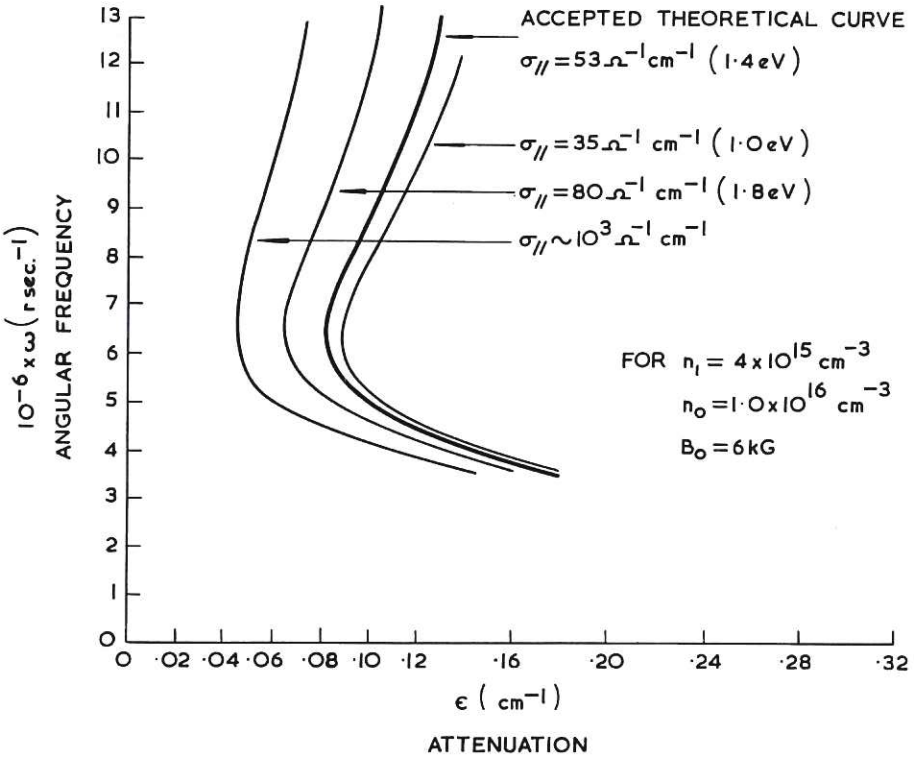

Fig. 10 (CLM-P72)

Wave damping - theoretical curves showing the dependence of ϵ, the attenuation coefficient, upon the conductivity σ, as a result of changes in T_e

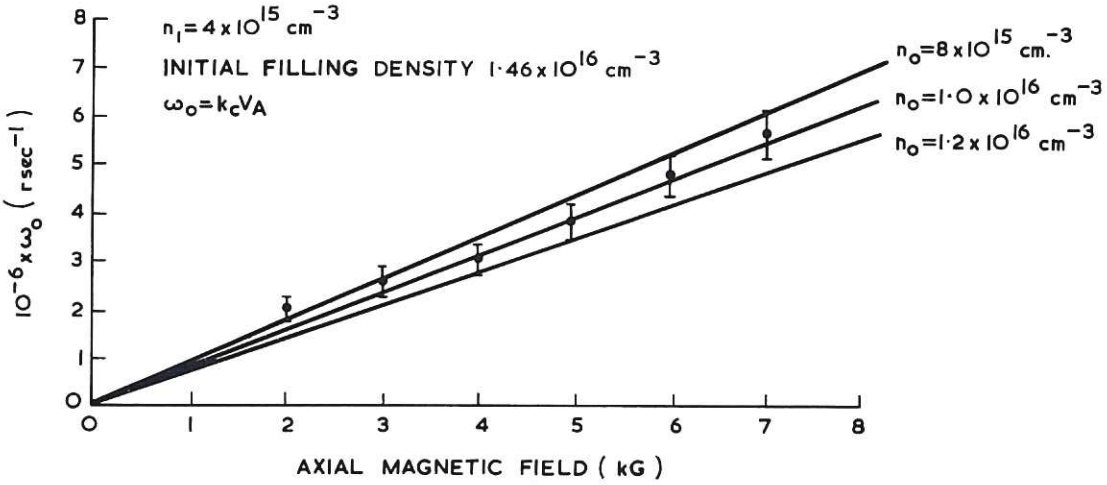

Fig. 11 (CLM-P72)

Variation of the lowest propagated (cut-off) frequency with applied magnetic field. Curves are drawn for three values of total particle density in the wave (n_o)